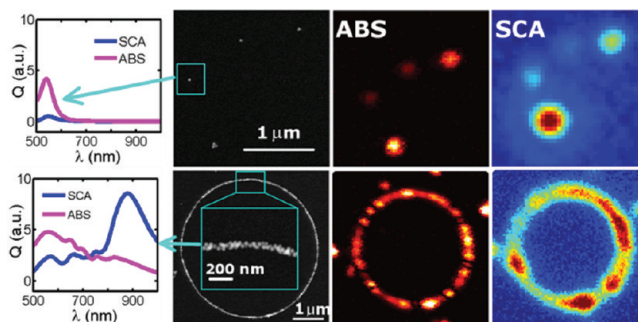# Radiative and Nonradiative Properties of Single Plasmonic Nanoparticles and Their Assemblies

WEI-SHUN CHANG,[†, §] BRITAIN WILLINGHAM,[†, §]
LIANE S. SLAUGHTER,[†, §] SERGIO DOMINGUEZ-MEDINA,[†, §]
PATTANAWIT SWANGLAP,[†, §] AND STEPHAN LINK[*, †, ‡, §]

[†]*Department of Chemistry, [‡]Department of Electrical and Computer Engineering,
and [§]Laboratory for Nanophotonics, Rice University, Houston,
Texas, United States*

RECEIVED ON DECEMBER 27, 2011

CONSPECTUS

A surface plasmon is the coherent oscillation of the conduction band electrons. When a metal nanoparticle is excited to produce surface plasmons, incident light is both scattered and absorbed, giving rise to brilliant colors. One available technique for measuring these processes, ensemble extinction spectroscopy, only measures the sum of scattering and absorption. Although the spectral responses of these processes are closely related, their relative efficiencies can differ significantly as a function of nanoparticle size and shape. For some applications, researchers may need techniques that can quantitatively measure absorption or scattering alone. Through advances in single particle spectroscopy, researchers can overcome this problem, separately determining the radiative (elastic and inelastic scattering) and nonradiative (absorption) properties of surface plasmons. Furthermore, because we can use the same sample preparation for both single particle spectroscopy measurements and electron microscopy, this technique provides detailed structural information and a direct correlation between optical properties and nanostructure morphology.

In this Account, we present our quantitative investigations of both radiative (scattering and one-photon luminescence) and nonradiative (absorption) properties of the same individual plasmonic nanostructures employing different single particle spectroscopy techniques. In particular, we have used a combined setup to study the same structure with dark-field scattering spectroscopy, photothermal heterodyne imaging, confocal luminescence microscopy, and scanning electron microscopy. While Mie theory thoroughly describes the overall size dependence of scattering and absorption for nanospheres, our real samples deviate significantly from the predicted trend: their particle shape is not perfectly spherical, especially when supported on a substrate. Because of the high excitation rate in laser based single particle measurements, we can efficiently detect one-photon luminescence despite a low quantum yield. For gold nanoparticles, the luminescence spectrum follows the scattering response, and therefore we assigned it to the emission of a plasmon. Due to strong near-field interactions the plasmonic response of closely spaced nanoparticles deviates significantly from that of the constituent nanoparticles. This response arises from coupled surface plasmon modes that combine those of the individual nanoparticles. Our correlated structural and optical imaging strategy is especially powerful for understanding these collective modes and their dependence on the assembly geometry.

Introduction

Localized surface plasmons, the collective oscillation of conduction band electrons, give rise to many unique optical phenomena in metallic nanoparticles.[1−4] However, long before plasmons were described theoretically by solutions to Maxwell's equations[5] or nanoparticles could be visualized directly using electron microscopy,[6] the vibrant color of noble metal nanoparticles attracted much attention and led to their early application in stained glasses. This color is due to both scattering and absorption of the incident light.[1−4] Figure 1 illustrates how scattering and absorption affect the appearance of a colloidal solution of
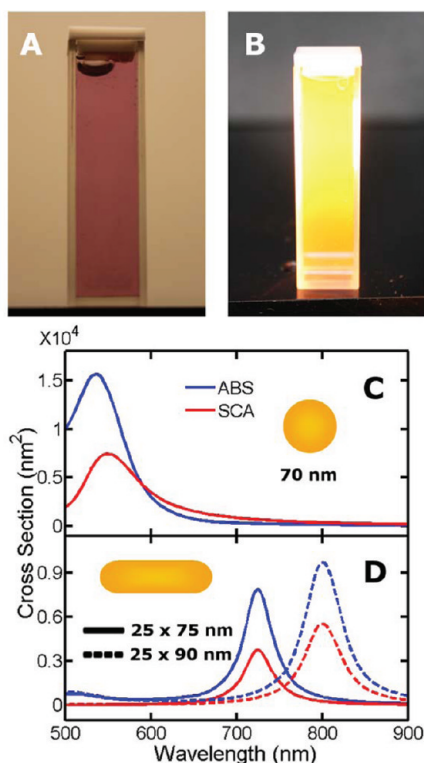
FIGURE 1. Transmittance (A) and reflectance (B) images of an aqueous solution of 70 nm AuNPs. Calculated absorption (blue) and scattering (red) spectra of 70 nm AuNPs (C) and AuNRs (D) with two different aspect ratios of 3 and 3.6.

70 nm spherical gold nanoparticles (AuNPs). If observed in transmission (A), the solution has a red color because of the absorption of green-yellow light. If instead the scattered light is viewed (B), the solution appears green-yellow. Consistent with the color in these images, the calculated scattering and absorption spectra in Figure 1C show a surface plasmon resonance (SPR) around 550 nm.

In addition to having a color that is distinctly different from the bulk metal, changes in nanoparticle size and shape produce vastly different plasmon modes,[7,8] which can furthermore be tailored through the interaction between closely spaced nanoparticles.[9,10] Figure 1D shows the scattering and absorption spectra of a gold nanorod (AuNR), which exhibits a red-shifted plasmon resonance polarized along the long AuNR axis. The maximum of this longitudinal SPR depends sensitively on the AuNR aspect ratio, exemplifying the extraordinary ability to tune the color by only varying the nanoparticle morphology without changing the chemical composition.[7,8]

While plasmon scattering and absorption are closely related, their spectral profiles and cross sections are not the same and vary with nanoparticle size and shape.[7,11]
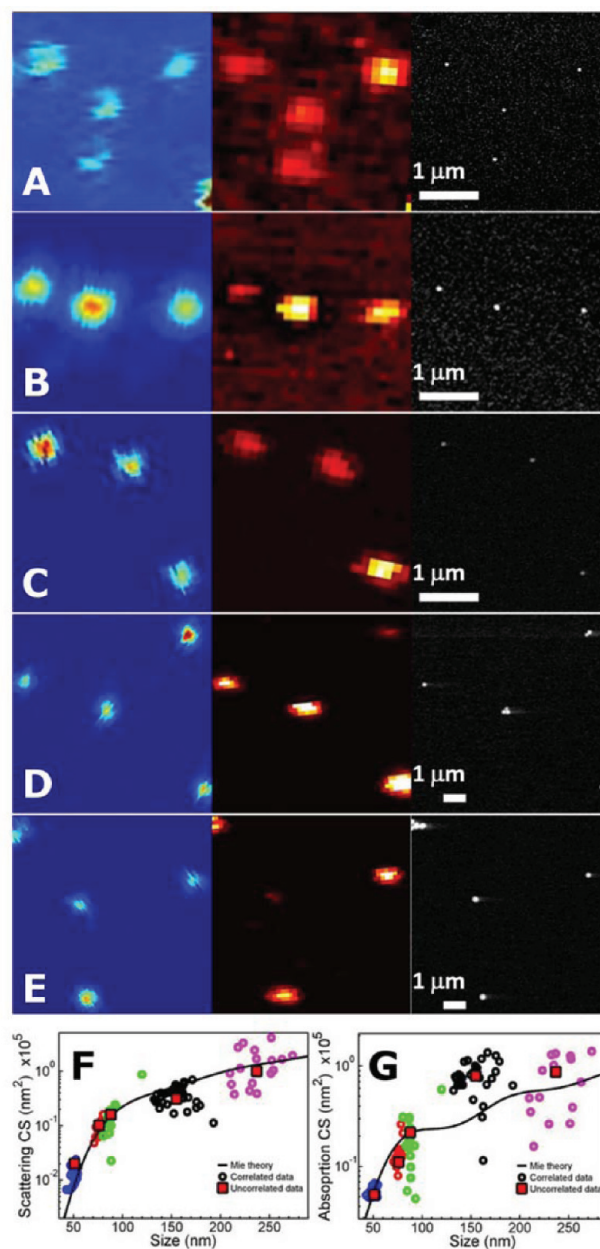

FIGURE 2. Size dependence of the scattering and absorption cross sections of AuNPs. Correlated scattering (left), absorption (center), and SEM (right) images of AuNPs for samples with mean diameters of 51 nm (A), 76 nm (B), 88 nm (C), 155 nm (D), and 237 nm (E). The intensity scale for the different images is arbitrary. With the size of an individual AuNP determined by SEM, the scattering and absorption cross sections at 532 nm are plotted as a function of AuNP diameter in (F) and (G), respectively. Trends predicted by Mie theory are given as solid black lines. Reprinted with permission from ref 11. Copyright 2010 American Chemical Society.

Apart from a fundamental understanding of these radiative (scattering) and nonradiative (absorption) properties, various applications are concerned with optimizing either of them or both. For example, in photothermal cancer therapy with metallic nanoparticles it is most

desirable to efficiently convert the incident radiation into heat,[12,13] while scattering is used for high contrast imaging.[12,14] Quantifying both scattering and absorption is therefore important for isolated as well as interacting metallic nanoparticles.

Measuring scattering and absorption properties separately is, however, not straightforward because typical UV−vis spectroscopy determines the extinction, which represents the total loss of the incident light and therefore corresponds to the sum of scattering and absorption. Combining extinction spectroscopy with other ensemble techniques such as angle-resolved reflectivity measurements[15] or photoacoustic spectroscopy[16] can in principle overcome this problem. It does not address the issue of spectral broadening though, which arises from the distribution of nanoparticle sizes, shapes, and environments, at least in samples of colloidal nanoparticles that are made by chemical synthesis.

Single particle spectroscopy has become an invaluable tool for overcoming issues caused by the heterogeneity in the morphology of nanoparticles[17−22] as well as in the spatial arrangement of assembled nanoparticles.[23−25] Although optical microscopy is limited by diffraction and therefore cannot resolve the structure of nanoparticles, it is possible to locate the same nanostructure as in an electron microscope (Figure 2).[11] Correlated electron microscopy and optical spectroscopy is an especially powerful approach for determining the plasmonic modes of strongly coupled metallic nanoparticles.[20] Furthermore, with the recent advances in measuring the absorption of single nanoparticles[26−29] and even molecules,[30] it has become possible to separately determine the radiative and nonradiative properties of individual plasmonic nanostructures. In this Account, we highlight our recent work on absorption, scattering, and luminescence of single AuNPs as well as AuNRs and one-dimensional assemblies of AuNPs.

Individual Nanoparticles

The plasmon scattering from individual metallic nanoparticles can be collected in a standard dark-field optical microscope,[11,14,17−25,31−37] in which the nanoparticles are excited with light incident at a larger angle while the scattered light is collected over a range of smaller angles. In contrast, a direct absorption measurement is difficult as it requires detection of a small signal on top of a large background intensity.[38,39] Several indirect techniques have been developed recently including photothermal heterodyne imaging,[26−29] which has been used extensively to probe

plasmonic nanostructures. In photothermal imaging, the SPR absorbs energy from a heating laser. The nonradiative decay of the plasmon oscillation causes a temperature increase of the nanoparticle and its environment, and therefore also a change in the temperature dependent refractive index of the surrounding medium. Modulating the intensity of the heating beam creates a refractive index variation that can be detected optically through interference with a second probe laser beam. Lock-in detection tuned to the laser modulation frequency makes this an extremely sensitive technique capable of imaging single metallic nanoparticles as small as 2 nm.[26]

Using both photothermal imaging and dark-field microscopy together with correlated scanning electron microscopy (SEM), we investigate the scattering and absorption cross sections of AuNPs as a function of size (Figure 2).[11] Five samples of AuNPs with mean diameters of 51 nm (A), 76 nm (B), 88 nm (C), 155 nm (D), and 237 nm (E) as determined separately by transmission electron microscopy are investigated at 532 nm. To be able to compare photothermal imaging carried out with a heating laser to scattering microscopy, the same laser instead of a white light lamp is coupled into a microscope employing a standard dark-field excitation and detection geometry. The images in Figure 2 demonstrate the correlation between the AuNPs observed by SEM (right column), absorption (middle column), and scattering (left column). Based on the local pattern visible in the images as well as large identification markers (not shown), the same AuNPs are uniquely identified. For a particular AuNP size identified in the SEM image, we therefore obtain the corresponding scattering and absorption intensities, which are plotted in Figures 2F and G, respectively. Each data point in these figures represents one AuNP, which is color coded according to the sample they originated from. In addition, average values (red squares) are included and are derived from distributions of scattering and absorption intensities of several hundred AuNPs, for which correlated SEM imaging is not carried out. The black lines are Mie theory calculations for the scattering and absorption cross sections at 532 nm for perfect spheres embedded in a medium with a homogeneous refractive index. Two important conclusions can be drawn from this data: (1) The overall experimental trend is well described by Mie theory and therefore validates our approach for separating scattering and absorption by dark-field microscopy and photothermal imaging. In particular for AuNPs smaller than ∼100 nm the absorption and scattering intensities scale as the volume and volume squared, respectively.[40] (2) For individual AuNPs,
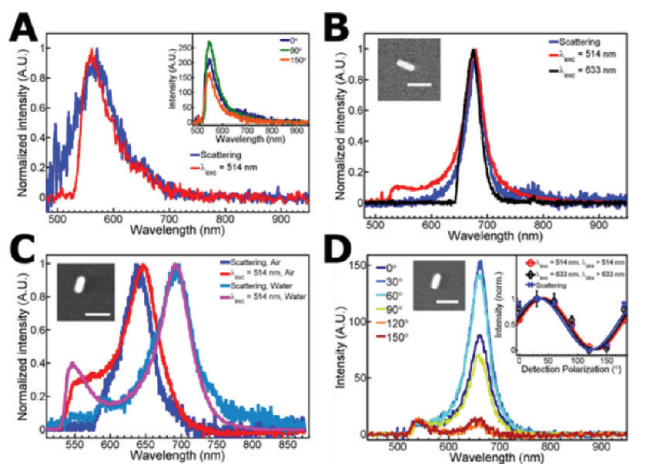
FIGURE 3. One-photon photoluminescence of single AuNPs and AuNRs. (A) Unpolarized scattering (blue) and 514 nm excited lumines-cence (red) spectra of a 45 nm diameter AuNP. The luminescence is weakly polarized (inset) as the AuNP is likely not perfectly spherical. (B) Unpolarized scattering (blue) and luminescence spectra excited at 514 nm (red) and 633 nm (black) for a AuNR. (C) Unpolarized scattering (blue and cyan) and 514 nm excited luminescence (red and magenta) spectra for a AuNR, recorded for two different refractive indices of the sur-rounding medium (air and water). (D) Polarized luminescence spectra of a AuNR with 514 nm excitation. The polarization dependence of the integrated luminescence excited at 514 nm (red) and 633 nm (black) follows the behavior for the scattering (blue) of the longitudinal plasmon resonance. All scale bars in the SEM images correspond to 100 nm. Reprinted with permission from ref 43. Copyright 2011 American Chemical Society.

FIGURE 4. Polarization-sensitive photothermal imaging of AuNRs. Correlated SEM (A) and photothermal (B) images recorded with circularly polarized 675 nm excitation light. By changing the polarization direc-tion of a linearly polarized excitation beam the polarization dependence of plasmon absorption is obtained for the two single AuNRs (C, D) and the dimer (E) highlighted in (A). The phase of the intensity modulation yields the orientation of the two AuNRs. Reprinted from ref 28. Copy-right 2010 National Academy of Sciences, USA.

the deviation from Mie theory can be very significant, which can be explained by the aspherical AuNP shape and the symmetry breaking by the glass substrate[18,37] as well as plasmonic interactions with the substrate through image charges.[33]

In addition to elastic scattering, which is usually assumed and we have referred to so far as well, inelastic scattering is also an important aspect of the radiative properties of plasmons. One- and two-photon excitation at a fixed fre-quency leads to luminescence in metallic nanoparticles. In particular, the origin of the weak one-photon luminescence has been assigned to different mechanisms, including the radiative recombination of interband electron–hole pairs amplified by the local surface field[41] or the emission of a plasmon.[42] Single particle studies on AuNPs and AuNRs convincingly show that the luminescence arises from plas-mon emission (Figure 3).[43] This is concluded from the match of the scattering and luminescence spectra of single AuNPs and AuNRs that are also imaged by SEM as shown in Figure 3A and B. For AuNRs, emission mainly occurs from the longitudinal SPR independent of excitation at 514 or 633 nm. Further evidence for this mechanism is provided by
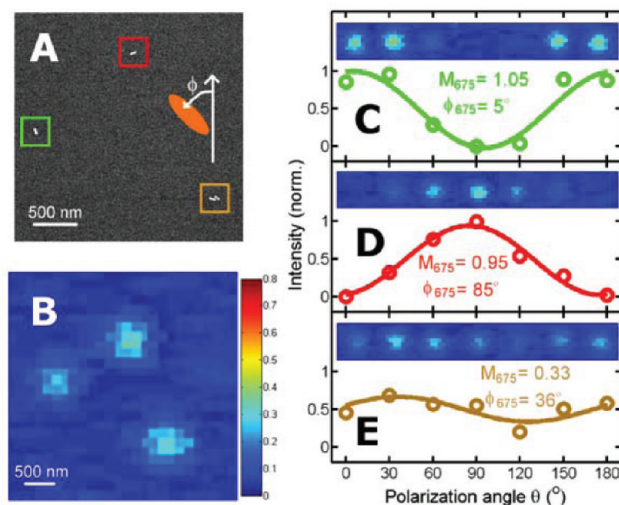
examining the dependence of the one-photon lumines-cence on the refractive index of the surrounding medium (Figure 3C). As the maximum of the SPR depends sensitively on the environment, a red-shift is observed for the scattering spectrum when the refractive index is increased by placing water on top of the sample. The luminescence spectrum shifts by the same amount. Finally, scattering from the longitudinal SPR is strongly polarized along the Au NR long axis (inset of Figure 3D). The luminescence for a single AuNR is equally polarized along the main AuNR axis. This is the case for both 514 and 633 nm excitation, which implies that a fast interconversion between electron–hole pairs and plasmons must be involved as absorption at 514 nm is polarized perpendicular to the AuNR with an underlying contribution of unpolarized interband transitions.[43]

The polarization dependence of the longitudinal SPR for a AuNR is not only a characteristic signature of the dipolar nature of this mode, but can also be used to determine the AuNR orientation by optical methods.[28,35,43] For scattering and luminescence, this is easily achieved by placing an analyzer in the detection path as was done for the data in Figure 3D. Note that for ensemble measurements of colloi-dal nanoparticle solutions, it is much harder to determine the polarization dependence of SPRs because the nano-particles are freely rotating in solution compared to being

immobilized for the single particle measurements. Photothermal imaging can also be adapted to yield the orientation of single AuNRs (Figure 4).[28] The two single AuNRs in the SEM image in Figure 4A are orientated almost orthogonal to each other. After identifying the same AuNRs by photothermal imaging using circularly polarized excitation (Figure 4B), the photothermal signal is recorded as a function of polarization of the now linearly polarized heating beam (Figures 4C, D, E).

In contrast to dark-field scattering spectroscopy, we find that it is possible to also determine the AuNR orientation by exciting the transverse SPR.[28] Because photothermal imaging scales only with the particle volume, it is more sensitive for smaller nanoparticles. The transverse mode, which corresponds to the smaller width of the AuNRs, can therefore be detected by photothermal imaging while it is often absent in dark-field scattering spectra. This fact is significant because it allows one to probe the orientation of individual AuNRs using a single laser wavelength as the transverse SPR is mostly insensitive to changes in AuNR aspect ratio and the dielectric constant of the surrounding medium.

One-Dimensional Nanoparticle Assemblies

Similar to how atoms combine to form molecules, plasmon modes on different nanoparticles can hybridize to form new collective modes.[2,24,31,34] The strength of these near-field plasmon interactions depends on the interparticle distance,[34] while the symmetry of the nanoparticle arrangement and of the fundamental modes determines if the hybridized modes possess a dipole moment and can couple strongly to light (bright modes) or have no dipole and remain optically inactive (dark modes).[31] Based on this concept, plasmonic molecules have been designed both by bottom-up assembly[32] of chemically prepared nanoparticles as well as by top-down methods.[44] Recent progress on this vastly expanding field has been reviewed in ref 2. Here, we will summarize some of the results of our work that has focused on linear chains of nanoparticles.

For a linear chain of nanoparticles, the lowest energy plasmon mode is polarized along the length of the chain and initially continuously red-shifts as the number N of nanoparticles is increased.[45,46] This mode is due to the in-phase longitudinal coupling of all nanoparticle plasmons and gives rise to a bright super-radiant mode. Once the chain becomes longer than ~10 nanoparticles, the red-shift starts to saturate as plasmon coupling drops off as d^{-3}, where d is the distance.[47] In contrast, plasmon coupling perpendicular to the nanoparticle chain leads to a blue-shift because of

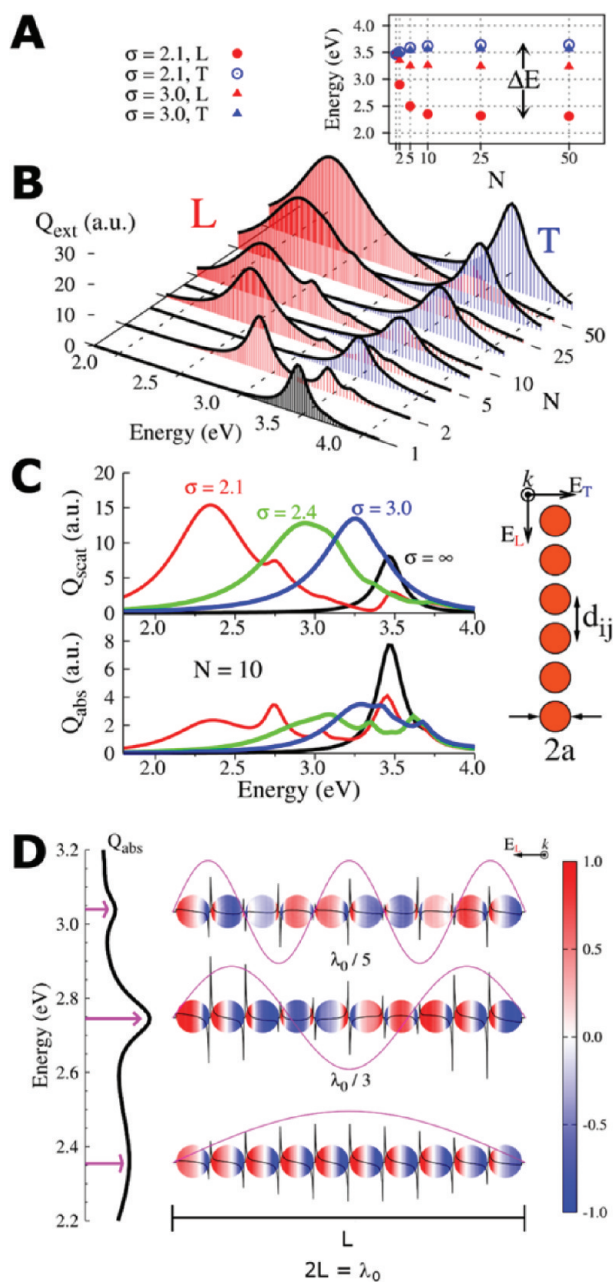**FIGURE 5.** Simulated scattering and absorption of finite chains of 50 nm silver nanoparticle with varying lengths and interparticle separations σ, defined by the ratio of the center-to-center separation and the radius. (A) Energy splitting ΔE between the longitudinal L (red) and transverse T (blue) dipole modes as a function of number of nanoparticles N for $\sigma = 2.1$ and $\sigma = 3.0$. (B) Extinction spectra of linear chains for varying N at $\sigma = 2.1$ with L and T incident polarization. (C) L-polarized scattering and absorption spectra of chains with $N = 10$ for different σ. (D) Surface charge density for a 10 nanoparticle chain with $\sigma = 2.1$. Standing waves of the polarization induced charge density, indicated by the magenta lines, have wavelengths of λ_0/n. The super-radiant and two bright subradiant modes for the corresponding absorption spectrum shown on the left are characterized by $n = 1$ and $n = 3, 5$. Reprinted with permission from ref 45. Copyright 2011 Optical Society of America.
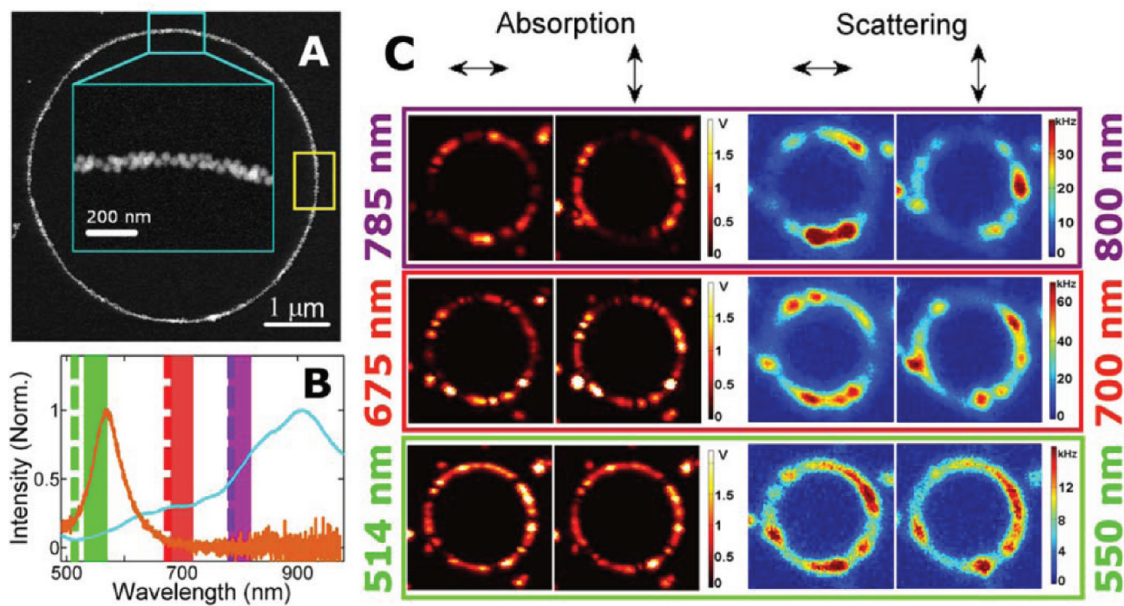
FIGURE 6. Scattering and absorption of collective plasmons in a self-assembled AuNP ring. (A) SEM image of a 4.6 μm ring composed of 40 nm AuNPs. (B) Unpolarized dark-field scattering spectra of the ring segment (cyan) marked by the cyan rectangle in (A) and a single AuNP (orange). The colored lines indicate the excitation wavelengths used for photothermal imaging (785, 675, and 514 nm) and for wavelength selective scattering imaging (800 ± 20, 700 ± 20, and 550 ± 20 nm). (C) Polarization-sensitive and wavelength dependent photothermal (left) and scattering (right) images acquired for the ring shown in (A). The excitation and detection wavelengths for absorption and scattering are displayed next to the images, while the polarization directions are given above the images. Reprinted from ref 50. Copyright 2011 National Academy of Sciences, USA.

antibonding interactions. The resulting energy splitting ΔE between the longitudinal and transverse polarized dipole resonances of the nanoparticle chain depends on the interparticle distance as illustrated in Figure 5A for finite chains of 50 nm silver nanoparticles with two interparticle separations of $\sigma = 2.1$ and $\sigma = 3.0$, where σ is the ratio of center-to-center distance and nanoparticle radius.[45] The corresponding spectra as a function of N for $\sigma = 2.1$ are shown in Figure 5B. These calculations are carried out using generalized Mie theory (GMT), considering up to 20 multipolar interactions, which is especially important for the closest nanoparticle separations.

In addition to the bright super-radiant mode, the closest interparticle distances facilitate the formation of subradiant and higher-order collective modes.[45,48,49] Figure 5C shows longitudinally polarized scattering and absorption spectra of chains with 10 silver nanoparticles for different interparticle separations.[45] As best seen from the absorption spectrum for $\sigma = 2.1$, two subradiant modes appear as resonances between the super-radiant mode at 2.35 eV and the quadrupole resonance at 3.47 eV. Figure 5D displays the corresponding surface charge density at the resonance energies of the super-radiant and these two subradiant modes.[45] In contrast to the super-radiant mode, the surface charge density of subradiant modes forms dipolelike domains that

alternate along the chain. For all modes, a standing wave pattern is visible in the surface charge density as indicated by the magenta line. The super-radiant mode can be assigned to a collective dipole antenna, whose wavelength λ_0 is equivalent to twice the chain length L. The subradiant modes identified in the spectra have wavelengths that are equal to odd integer fractions of λ_0 and are optically bright because their overall dipole moment is nonzero. There are also subradiant modes that are characterized by even integer fractions of λ_0, but they do not couple to light due to a zero dipole moment and therefore are dark. Losses for both bright and dark subradiant plasmon modes are minimized because of their reduced dipole moments. This can be exploited for energy propagation along nanoparticle chains and we find that excitation at energies corresponding to subradiant plasmon modes indeed yields the longest propagation distances, which can reach up to 3 μm for a perfectly ordered linear chain of 100 nm silver spheres that are separated by 5 nm ($\sigma = 2.1$).[45]

As the results in Figure 5 show, strongest plasmon coupling is achieved for the closest interparticle distances. To examine this regime experimentally for a collection of many nanoparticles, we have studied the scattering and absorption properties of nanoparticle assemblies that were prepared from the bottom-up.[50] Figure 6A shows an SEM image
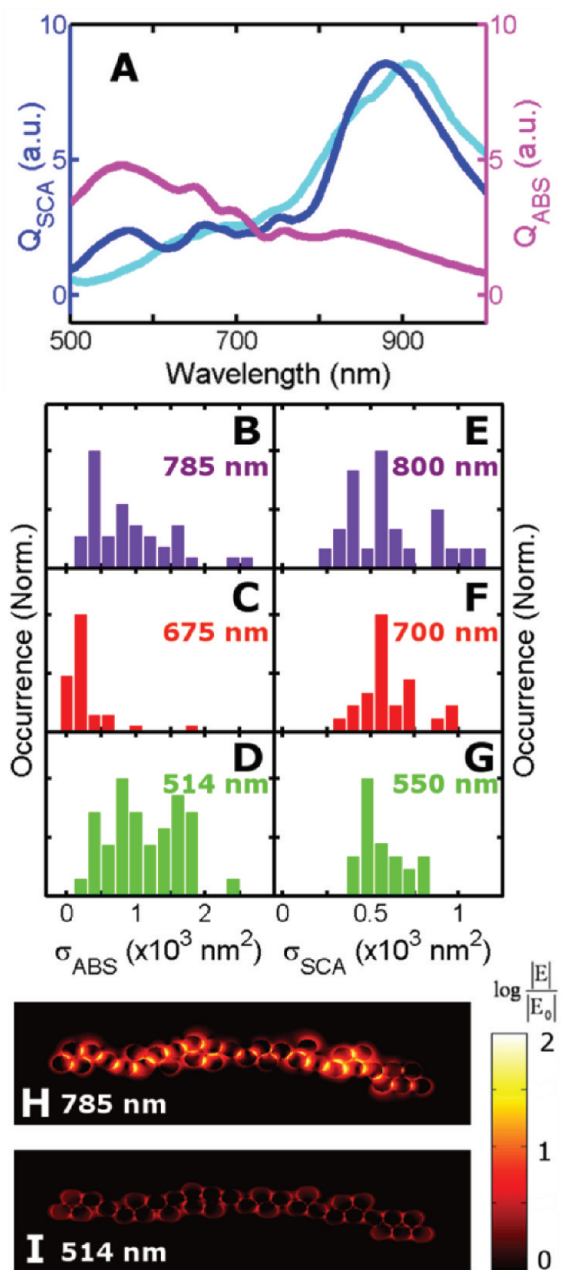
FIGURE 7. Scattering and absorption cross sections for a AuNP ring. (A) Unpolarized absorption (magenta) and scattering (blue) spectra of the ring segment marked by the cyan rectangle in Figure 6A are simulated using GMT. For comparison, the experimental scattering spectrum (cyan) from Figure 6B is also included. (B–D) Histograms of absorption cross sections obtained from 40 ring segments of the photothermal images for 785, 675, and 514 nm with circularly polarized excitation. (E–G) Histograms of scattering cross sections obtained from 24 ring segments of the scattering images measured with band-pass filters of 800 ± 20, 700 ± 20, and 550 ± 20 nm for unpolarized detection. Quantitative cross sections are obtained by comparison to individual AuNPs. Electromagnetic field enhancements (longitudinal polarization) of the same ring segment for 785 and 514 nm are given in (H) and (I). Reprinted from ref 50. Copyright 2011 National Academy of Sciences, USA.

of a ring that is composed of 40 nm AuNPs. Because of the large ring diameter of 4.6 μm, a local ring segment, as

illustrated by the higher magnification inset, represents a quasi one-dimensional chain of AuNPs with interparticle separations of only a few nanometers. The straightforward assembly at the interface between water droplets and an organic solvent furthermore makes such rings adequate systems for investigating the plasmonic properties in strongly coupled one-dimensional structures. The dark-field scattering spectrum (cyan) of the highlighted ring segment is displayed in Figure 6B and is acquired using a pinhole in the detection path to isolate the signal from only this region. Compared to the scattering spectrum of a single constituent AuNP (orange), the collective plasmon response is characterized by several red-shifted modes that are highly polarized tangential to the ring circumference and hence parallel to the local segment. This is best seen in the wavelength and polarization resolved scattering and absorption images in Figure 6C. The polarization anisotropy decreases at shorter wavelength as higher-order longitudinal as well as transverse plasmon modes are excited.

The photothermal images in Figure 6C clearly demonstrate that plasmon coupling also leads to nonradiative modes at wavelengths red-shifted from the constituent AuNP resonance. To better understand the spectral features of the ring segment and to analyze the relative contributions of scattering and absorption, the optical response is modeled based on the AuNP arrangement obtained from SEM images.[50] Figure 7A displays the simulated scattering and absorption spectra of the ring segment highlighted in Figure 6A. The agreement with the experimental scattering spectrum is excellent and allows us to assign the resonance around 900 nm to the super-radiant mode. Furthermore, consistent with the observed polarization anisotropy, the three selected wavelength regions in Figure 6C can be assigned as follows: (1) at 785/800 nm a combination of the dipole mode and the first higher-order mode are excited, (2) at 675/700 nm only higher-order longitudinal modes are excited, and (3) at 514/550 nm both higher-order longitudinal as well as transverse modes are excited.

For the super-radiant plasmon mode, scattering dominates over absorption as seen in Figure 7A, which is also in agreement with the calculations shown for the silver nanoparticle chains in Figure 5C. On the other hand, at the single AuNP plasmon resonance, absorption is larger than scattering. To probe this trend experimentally, Figure 7B–G compares the absorption (Figure 7B–D) and scattering (Figure 7E–G) cross section determined along the ring from wavelength resolved images. The intensity hot spots in both scattering and absorption images (Figure 6C) cause a
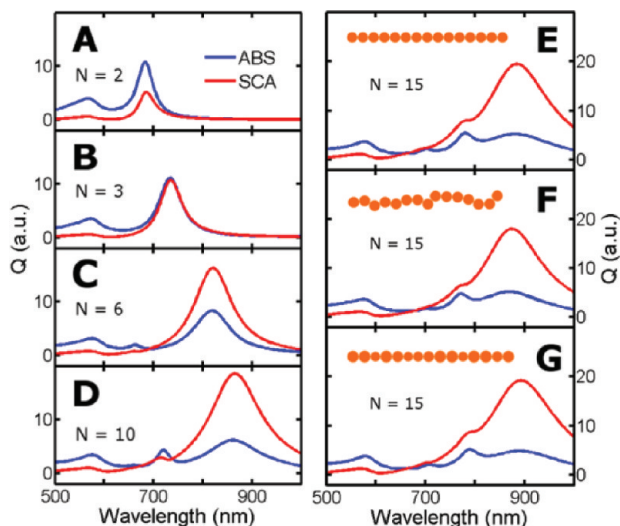
FIGURE 8. Simulated absorption (blue) and scattering (red) spectra of linear AuNP chains for longitudinal incident polarization. The number of AuNPs N is varied from 2 (A), 3 (B), 6 (C), to 10 (D). The AuNPs are 40 nm in diameter and the surface-to-surface separation is constant at 1 nm. The effect of disorder is evaluated in (E–G) for chains with $N = 15$. Compared to the perfectly ordered linear chain (E), displacing the AuNPs in the perpendicular direction (F) or introducing a distribution of nanoparticle sizes (G) produces only small changes in the scattering and absorption spectra.

distribution of intensity values. Nevertheless, the overall trend of a decreasing absorption and increasing scattering cross section with increasing wavelength is reproduced. Lower absorption losses at the super-radiant mode benefit antenna-type applications that take advantage of coupling light to nanoscale areas with strongly increased electromagnetic field enhancements at the lowest energy resonance, as is illustrated in the comparison of electric field maps calculated at 785 (Figure 7H) and 514 (Figure 7I) nm.

We have argued that these AuNP rings are large enough so that the plasmonic properties are essentially described by local one-dimensional segments. As shown for the silver nanoparticle chains, the maximum of the super-radiant modes stops red-shifting significantly for chains with 10 or more nanoparticles. This is also the case for the 40 nm AuNPs that comprise the rings, as illustrated in Figure 8A–E, which shows the longitudinally polarized scattering and absorption spectra of perfectly linear chains with 1 nm gaps as a function of chain length. The absorption spectra again clearly show the appearance of a subradiant mode on the high energy side of the super-radiant mode. These GMT calculations furthermore allow us to address the influence of disorder on the plasmonic response. This is especially important for assemblies created from the bottom up, such as the Au NP rings, because variations of nanoparticle size, shape, and arrangement cannot be

avoided. In Figure 8E–G, we plot the scattering and absorption spectra of a perfectly ordered linear chain made from 15 AuNPs (Figure 8E), compared to a chain where the AuNPs are randomly displaced in the transverse direction by as much as a nanoparticle diameter (Figure 8F), and a chain with a random variation in nanoparticle size between 35 and 45 nm (Figure 8G) based on the experimental size distribution. The spectral shift for the super-radiant mode for these three cases is less than 20 nm, demonstrating that for a significantly long chain disorder in nanoparticle positioning and size has only a small overall effect on the plasmonic properties. This is in contrast to smaller nanoparticle assemblies because for those assemblies each nanoparticle carries a proportionally larger weight to each hybridized mode. In addition, although disorder breaks the symmetry of the system and therefore lifts the degeneracy of the coupled plasmon modes, the associated spectral shifts are small compared to the width of each mode in large and hence retarded assemblies, thereby effectively masking the effect of disorder on the collective plasmon scattering and absorption.

Conclusions and Outlook

In this Account, we have discussed the radiative and nonradiative properties of plasmonic nanoparticles and their assemblies. Single particle spectroscopy techniques, especially when correlated with SEM imaging, allow one to separately determine the size and shape dependent plasmon scattering and absorption. A combined structural imaging and optical spectroscopy approach is particularly useful for understanding the plasmonic response of strongly coupled nanoparticle assemblies, which are prepared by bottom-up techniques and hence are prone to disorder. As discussed here for chains, the effect of disorder on the collective plasmon modes decreases as the assembly grows in size. Just as oligomers are treated as molecules, nanoparticle chains can be thought of as plasmonic polymers. Our future work is focused on fabricating well-defined linear nanoparticle assemblies to further elucidate the dependence of the optical properties of plasmonic polymers on such variables as chain length, repeat unit, and degree of disorder.

BIOGRAPHICAL INFORMATION

Wei-Shun Chang is a postdoctoral researcher. He received his Ph.D. from UT Austin (2007) with Paul Barbara. His current research interests are the radiative and nonradiative properties of strongly coupled plasmons in nanoparticle assemblies.

Britain Willingham is a Ph.D. candidate in applied physics. His research interests include mathematical physics, quantum chemistry, classical field theory, numerical techniques in electrodynamic modeling, nanophotonics, and plasmonics.

Liane S. Slaughter is a Ph.D. candidate in chemistry. She received her B.A. in chemistry from Cornell University in 2007. Her research interests include self-assembly and the properties of self-assembled nanoparticles.

Sergio Dominguez-Medina is a graduate student in chemistry. He received his B.S. from Tecnológico de Monterrey in 2009. His current research interests include nanoparticle diffusion and nanoparticle−protein interactions.

Pattanawit Swanglap is a Ph.D. candidate in chemistry. He received his B.S. in chemistry from Silpakorn University, Thailand, in 2008. His research interests include the active control of plasmon resonances.

Stephan Link is an assistant professor in the Departments of Chemistry and Electrical and Computer Engineering at Rice University. He received his Ph.D. from Georgia Tech (2000) working with Mostafa El-Sayed and performed postdoctoral research with Paul Barbara at UT Austin. The main interest of his research group is the study of the optical properties of plasmonic nanomaterials.

FOOTNOTES

REFERENCES

1 Bohren, C. F.; Huffman, D. R. *Absorption and Scattering of Light by Small Particles*; John Wiley and Sons, Inc.: New York, 1983.

2 Halas, N. J.; Lal, S.; Chang, W.-S.; Link, S.; Nordlander, P. Plasmons in Strongly Coupled Metallic Nanostructures. *Chem. Rev.* **2011**, *111*, 3913–3961.

3 Kreibig, U.; Vollmer, M. *Optical Properties of Metal Clusters*; Springer: Berlin, 1995.

4 Maier, S. A. *Plasmonics: Fundamentals and Applications*; Springer: New York, 2007.

5 Mie, G. Beiträge zur Optik trüber Medien, speziell kolloidaler Metallösungen. *Ann. Phys.* **1908**, *25*, 377–445.

6 Dusemund, B.; Hoffmann, A.; Salzmann, T.; Kreibig, U.; Schmid, G. Cluster matter: the transition of optical elastic scattering to regular reflection. *Z. Phys. D: At., Mol. Clusters* **1991**, *20*, 305–308.

7 Jain, P. K.; Lee, K. S.; El-Sayed, I. H.; El-Sayed, M. A. Calculated absorption and scattering properties of gold nanoparticles of different size, shape, and composition: Applications in biological imaging and biomedicine. *J. Phys. Chem. B* **2006**, *110*, 7238–7248.

8 Link, S.; El-Sayed, M. A. Shape and size dependence of radiative, non-radiative and photothermal properties of gold nanocrystals. *Int. Rev. Phys. Chem.* **2000**, *19*, 409–453.

9 Mirkin, C. A.; Letsinger, R. L.; Mucic, R. C.; Storhoff, J. J. A DNA-based method for rationally assembling nanoparticles into macroscopic materials. *Nature* **1996**, *382*, 607–609.

10 Landes, C. F.; Link, S.; Mohamed, M. B.; Nikoobakht, B.; El-Sayed, M. A. Some properties of spherical and rod-shaped semiconductor and metal nanocrystals. *Pure Appl. Chem.* **2002**, *74*, 1675–1692.

11 Tcherniak, A.; Ha, J. W.; Dominguez-Medina, S.; Slaughter, L. S.; Link, S. Probing a Century Old Prediction One Plasmonic Particle at a Time. *Nano Lett.* **2010**, *10*, 1398–1404.

12 Huang, X.; El-Sayed, I. H.; Qian, W.; El-Sayed, M. A. Cancer Cell Imaging and Photothermal Therapy in the Near-Infrared Region by Using Gold Nanorods. *J. Am. Chem. Soc.* **2006**, *128*, 2115–2120.

13 Loo, C.; Lowery, A.; Halas, N.; West, J.; Drezek, R. Immunotargeted Nanoshells for Integrated Cancer Imaging and Therapy. *Nano Lett.* **2005**, *5*, 709–711.

14 Schultz, S.; Smith, D. R.; Mock, J. J.; Schultz, D. A. Single-target molecule detection with nonbleaching multicolor optical immunolabels. *Proc. Natl. Acad. Sci. U.S.A.* **2000**, *97*, 996–1001.

15 Langhammer, C.; Kasemo, B.; Zoric, I. Absorption and scattering of light by Pt, Pd, Ag, and Au nanodisks: Absolute cross sections and branching ratios. *J. Chem. Phys.* **2007**, *126*, 194702.

16 Cho, E. C.; Kim, C.; Zhou, F.; Cobley, C. M.; Song, K. H.; Chen, J.; Li, Z.-Y.; Wang, L. V.; Xia, Y. Measuring the Optical Absorption Cross Sections of Au-Ag Nanocages and Au Nanorods by Photoacoustic Imaging. *J. Phys. Chem. C* **2009**, *113*, 9023–9028.

17 Au, L.; Chen, Y.; Zhou, F.; Camargo, P.; Lim, B.; Li, Z.-Y.; Ginger, D.; Xia, Y. Synthesis and optical properties of cubic gold nanoframes. *Nano Res.* **2008**, *1*, 441–449.

18 Hu, M.; Chen, J.; Marquez, M.; Xia, Y.; Hartland, G. V. Correlated Rayleigh Scattering Spectroscopy and Scanning Electron Microscopy Studies of Au-Ag Bimetallic Nanoboxes and Nanocages. *J. Phys. Chem. C* **2007**, *111*, 12558–12565.

19 Sherry, L. J.; Jin, R.; Mirkin, C. A.; Schatz, G. C.; Van Duyne, R. P. Localized Surface Plasmon Resonance Spectroscopy of Single Silver Triangular Nanoprisms. *Nano Lett.* **2006**, *6*, 2060–2065.

20 Slaughter, L.; Chang, W.-S.; Link, S. Characterizing Plasmons in Nanoparticles and Their Assemblies with Single Particle Spectroscopy. *J. Phys. Chem. Lett.* **2011**, *2*, 2015–2023.

21 Slaughter, L. S.; Chang, W.-S.; Swanglap, P.; Tcherniak, A.; Khanal, B. P.; Zubarev, E. R.; Link, S. Single-Particle Spectroscopy of Gold Nanorods beyond the Quasi-Static Limit: Varying the Width at Constant Aspect Ratio. *J. Phys. Chem. C* **2010**, *114*, 4934–4938.

22 Nehl, C. L.; Liao, H. W.; Hafner, J. H. Optical properties of star-shaped gold nanoparticles. *Nano Lett.* **2006**, *6*, 683–688.

23 Chang, W. S.; Slaughter, L. S.; Khanal, B. P.; Manna, P.; Zubarev, E. R.; Link, S. One-Dimensional Coupling of Gold Nanoparticle Plasmons in Self-Assembled Ring Super-structures. *Nano Lett.* **2009**, *9*, 1152–1157.

24 Barrow, S. J.; Funston, A. M.; Gomez, D. E.; Davis, T. J.; Mulvaney, P. Surface Plasmon Resonances in Strongly Coupled Gold Nanosphere Chains from Monomer to Hexamer. *Nano Lett.* **2011**, *11*, 4180–4187.

25 Lee, J.; Hasan, W.; Lee, M. H.; Odom, T. W. Optical Properties and Magnetic Manipulation of Bimaterial Nanopyramids. *Adv. Mater.* **2007**, *19*, 4387–4391.

26 Berciaud, S.; Cognet, L.; Blab, G. A.; Lounis, B. Photothermal heterodyne imaging of individual nonfluorescent nanoclusters and nanocrystals. *Phys. Rev. Lett.* **2004**, *93*, 257402/1–4.

27 Boyer, D.; Tamarat, P.; Maali, A.; Lounis, B.; Orrit, M. Photothermal imaging of nanometer-sized metal particles among scatterers. *Science* **2002**, *297*, 1160–1163.

28 Chang, W.-S.; Ha, J. W.; Slaughter, L. S.; Link, S. Plasmonic nanorod absorbers as orientation sensors. *Proc. Natl. Acad. Sci. U.S.A.* **2010**, *107*, 2781–2786.

29 Gaiduk, A.; Ruijgrok, P. V.; Yorulmaz, M.; Orrit, M. Detection limits in photothermal microscopy. *Chem. Sci.* **2010**, *1*, 343–350.

30 Gaiduk, A.; Yorulmaz, M.; Ruijgrok, P. V.; Orrit, M. Room-Temperature Detection of a Single Molecule's Absorption by Photothermal Contrast. *Science* **2010**, *330*, 353–356.

31 Brown, L. V.; Sobhani, H.; Lassiter, J. B.; Nordlander, P.; Halas, N. J. Heterodimers: Plasmonic Properties of Mismatched Nanoparticle Pairs. *ACS Nano* **2010**, *4*, 819–832.

32 Fan, J. A.; Wu, C. H.; Bao, K.; Bao, J. M.; Bardhan, R.; Halas, N. J.; Manoharan, V. N.; Nordlander, P.; Shvets, G.; Capasso, F. Self-Assembled Plasmonic Nanoparticle Clusters. *Science* **2010**, *328*, 1135–1138.

33 Knight, M. W.; Wu, Y.; Lassiter, J. B.; Nordlander, P.; Halas, N. J. Substrates Matter: Influence of an Adjacent Dielectric on an Individual Plasmonic Nanoparticle. *Nano Lett.* **2009**, *9*, 2188–2192.

34 Slaughter, L. S.; Wu, Y.; Willingham, B. A.; Nordlander, P.; Link, S. Effects of Symmetry Breaking and Conductive Contact on the Plasmon Coupling in Gold Nanorod Dimers. *ACS Nano* **2010**, *4*, 4657–4666.

35 Sonnichsen, C.; Alivisatos, A. P. Gold nanorods as novel nonbleaching plasmon-based orientation sensors for polarized single-particle microscopy. *Nano Lett.* **2005**, *5*, 301–304.

36 Sonnichsen, C.; Franzl, T.; Wilk, T.; von Plessen, G.; Feldmann, J.; Wilson, O.; Mulvaney, P. Drastic reduction of plasmon damping in gold nanorods. *Phys. Rev. Lett.* **2002**, *88*, 077402/1–4.

37 Sherry, L. J.; Chang, S.-H.; Schatz, G. C.; Van Duyne, R. P.; Wiley, B. J.; Xia, Y. Localized Surface Plasmon Resonance Spectroscopy of Single Silver Nanocubes. *Nano Lett.* **2005**, *5*, 2034–2038.

38 Celebrano, M.; Kukura, P.; Renn, A.; Sandoghdar, V. Single-molecule imaging by optical absorption. *Nat. Photonics* **2011**, *5*, 95–98.

39 Hong, X.; van Dijk, E. M. P. H; Hall, S. R.; Gotte, J. B.; van Hulst, N. F.; Gersen, H. Background-Free Detection of Single 5 nm Nanoparticles through Interferometric Cross-Polarization Microscopy. *Nano Lett.* **2011**, *11*, 541–547.

40 van Dijk, M. A.; Tchebotareva, A. L.; Orrit, M.; Lippitz, M.; Berciaud, S.; Lasne, D.; Cognet, L.; Lounis, B. Absorption and scattering microscopy of single metal nanoparticles. *Phys. Chem. Chem. Phys.* **2006**, *8*, 3486–3495.

41 Varnavski, O. P.; Goodson, T., III; Mohamed, M. B.; El-Sayed, M. A. Femtosecond excitation dynamics in gold nanospheres and nanorods. *Phys. Rev. B* **2005**, *72*, 235405.

42 Dulkeith, E.; Niedereichholz, T.; Klar, T. A.; Feldmann, J.; von Plessen, G.; Gittins, D. I.; Mayya, K. S.; Caruso, F. Plasmon emission in photoexcited gold nanoparticles. *Phys. Rev. B* **2004**, *70*, 205424.

43 Tcherniak, A.; Dominguez-Medina, S.; Chang, W.-S.; Swanglap, P.; Slaughter, L. S.; Landes, C. F.; Link, S. One-Photon Plasmon Luminescence and Its Application to Correlation Spectroscopy as a Probe for Rotational and Translational Dynamics of Gold Nanorods. *J. Phys. Chem. C* **2011**, *115*, 15938–15949.

44 Hentschel, M.; Saliba, M.; Vogelgesang, R.; Giessen, H.; Alivisatos, A. P.; Liu, N. Transition from Isolated to Collective Modes in Plasmonic Oligomers. *Nano Lett.* **2010**, *10*, 2721–2726.

45 Willingham, B.; Link, S. Energy transport in metal nanoparticle chains via sub-radiant plasmon modes. *Opt. Express* **2011**, *19*, 6450–6461.

46 Citrin, D. S. Plasmon Polaritons in Finite-Length Metal: Nanoparticle Chains: The Role of Chain Length Unravelled. *Nano Lett.* **2005**, *5*, 985–989.

47 Maier, S. A.; Brongersma, M. L.; Kik, P. G.; Atwater, H. A. Observation of near-field coupling in metal nanoparticle chains using far-field polarization spectroscopy. *Phys. Rev. B* **2002**, *65*, 193408.

48 Liu, M.; Lee, T.-W.; Gray, S. K.; Guyot-Sionnest, P.; Pelton, M. Excitation of Dark Plasmons in Metal Nanoparticles by a Localized Emitter. *Phys. Rev. Lett.* **2009**, *102*, 107401.

49 Stockman, M. I. Nanoscience: Dark-hot resonances. *Nature* **2010**, *467*, 541–542.

50 Chang, W.-S.; Willingham, B. A.; Slaughter, L. S.; Khanal, B. P.; Vigderman, L.; Zubarev, E. R.; Link, S. Low absorption losses of strongly coupled surface plasmons in nanoparticle assemblies. *Proc. Natl. Acad. Sci. U.S.A.* **2011**, *108*, 19879–19884.